

Article

An Embryonic Zebrafish Model to Screen Disruption of Gut-Vascular Barrier upon Exposure to Ambient Ultrafine Particles

Kyung In Baek ^{1,†} , Yi Qian ^{1,2,†} , Chih-Chiang Chang ¹, Ryan O'Donnell ¹, Ehsan Soleimani ³, Constantinos Sioutas ³ , Rongsong Li ⁴ and Tzung K. Hsiai ^{1,5,6,*}

¹ Department of Bioengineering and Medicine, University of California, Los Angeles, CA 90095, USA; qorruddls122@gmail.com (K.I.B.); iqiany1614@zju.edu.cn (Y.Q.); changc4@ucla.edu (C.-C.C.); ROdonnell@mednet.ucla.edu (R.O.)

² Department of Cardiology, The Second Affiliated Hospital, School of Medicine, Zhejiang University, Hangzhou 310027, China

³ Department of Civil and Environmental Engineering, University of Southern California, Los Angeles, CA 90089, USA; ehsansol@usc.edu (E.S.); sioutas@usc.edu (C.S.)

⁴ College of Health Sciences and Environmental Engineering, Shenzhen Technology University, Shenzhen 518118, China; lirongsong@sztu.edu.cn

⁵ Division of Cardiology, Department of Medicine, School of Medicine, University of California, Los Angeles, CA 90095, USA

⁶ Veterans Affairs Greater Los Angeles Healthcare System, Department of Medicine, Los Angeles, CA 90073, USA

* Correspondence: thsiai@mednet.ucla.edu; Tel.: +1-310-268-3839

† Equally contributed.

Received: 29 October 2020; Accepted: 17 November 2020; Published: 19 November 2020



Abstract: Epidemiological studies have linked exposure to ambient particulate matter (PM) with gastrointestinal (GI) diseases. Ambient ultrafine particles (UFP) are the redox-active sub-fraction of PM_{2.5}, harboring elemental and polycyclic aromatic hydrocarbons from urban environmental sources including diesel and gasoline exhausts. The gut-vascular barrier (GVB) regulates paracellular trafficking and systemic dissemination of ingested microbes and toxins. Here, we posit that acute UFP ingestion disrupts the integrity of the intestinal barrier by modulating intestinal Notch activation. Using zebrafish embryos, we performed micro-gavage with the fluorescein isothiocyanate (FITC)-conjugated dextran (FD10, 10 kDa) to assess the disruption of GVB integrity upon UFP exposure. Following micro-gavage, FD10 retained in the embryonic GI system, migrated through the cloaca. Conversely, co-gavaging UFP increased transmigration of FD10 across the intestinal barrier, and FD10 fluorescence occurred in the venous capillary plexus. Ingestion of UFP further impaired the mid-intestine morphology. We performed micro-angiogram of FD10 to corroborate acute UFP-mediated disruption of GVB. Transient genetic and pharmacologic manipulations of global Notch activity suggested Notch regulation of the GVB. Overall, our integration of a genetically tractable embryonic zebrafish and micro-gavage technique provided epigenetic insights underlying ambient UFP ingestion disrupts the GVB.

Keywords: ultrafine particles; zebrafish; micro-gavage; Notch signaling; gut-vascular barrier

1. Introduction

Ultrafine particles (UFP, $d_p < 0.1$ to $0.2 \mu\text{m}$ in diameter), comprised of a mixture of heavy transition metals and redox cycling organic chemicals, are redox-active components of ambient particulate matter

(PM, $d_p < 2.5 \mu\text{m}$) [1,2]. Recent epidemiological studies have supported the link between UFP exposure and gastrointestinal (GI) diseases such as inflammatory bowel disease [3]. While the cardiopulmonary system remains the main entry point for ambient UFP exposure, UFP are orally ingested via contaminated food and water supplies for intestinal pro-inflammatory potentials [4–7]. Dietary UFP, including titanium dioxide nanoparticles used as food additives and aluminosilicate minerals in drinking water, are absorbed by intestinal epithelial lymphocytes, potentiating pro-inflammatory cytokines and T-cell proliferation [8,9]. Inhaled UFP increases colonic inflammation and facilitates intestinal release of fatty acids and pro-inflammatory mediators as a result of bronchial mucociliary removal to the oropharynx [10]. While intestinal inflammatory responses suppress mucosal stability and subsequent integrity of the intestinal epithelial barrier, the epigenetic cues underlying ambient UFP exposure and the barrier integrity remain elusive [11].

The gut-vascular barrier (GVB) constitutes both intestinal epithelial and vascular endothelial barriers that regulate dissemination of microbes and toxins from the intestinal tract to systemic circulation [12–14]. Analogous to the blood–brain barrier, a layer of endothelial cells along with surrounding glial cells and pericytes, the GVB develops cellular junctions to form a functional barrier, regulating paracellular trafficking (<4 kDa) into the vascular endolumen [13,14]. Junctional complexes in an endothelial layer including tight junctions (TJ), occludin, zonula occludens-1 (ZO-1), claudin, and adherens proteins, including vascular endothelial-cadherin and β -catenin characterize the integrity of the GVB. Furthermore, complementary mechanisms of endothelial transcytosis and GVB homeostasis share similarities with the blood–brain barrier [15]. Microbial pathogens such as *Salmonella typhimurium* or celiac dysbiosis modulate the Wnt3a/ β -catenin signaling pathway to reduce enteric TJ expression, and dismantle the GVB for diffusion of intestinal pro-inflammatory mediators [14,16]. While acute UFP exposure is reported to increase both colonic epithelial and endothelial permeability in vitro (24–48 h), in conjunction with an altered diversity of gut microbiota in low density lipoprotein receptor-null mice (*ldlr*^{-/-}, 10 weeks), the molecular cues whereby UFP ingestion disrupts the GVB remain elusive [10,17,18].

In this context, we posit that acute UFP ingestion via micro-gavage disrupts the GVB by inhibiting Notch-dependent TJ expression. To visualize disruption of the GVB, we sought to use the embryonic zebrafish (*Danio rerio*) model for its transparent anatomical features and conserved genetic systems during organogenesis, and short developmental cycle that facilitates high-throughput pharmacogenetic analysis for novel therapeutic targets [19]. By using transgenic Tg(*flk1*: mcherry) zebrafish embryos, we demonstrated a micro-gavage technique in order to deliver UFP directly to the embryonic intestinal bulbs for rapid screening the disruption of the GVB. In FITC-conjugated dextran (FD10, 10 kDa)-gavaged controls, FD10 remained in the intestinal bulbs and the mid-intestine migrating only through the cloaca. At 7 h post gavage (hpg), co-gavaging UFP (25–50 $\mu\text{g}\cdot\text{mL}^{-1}$) attenuated the intestinal barrier and global development of the GI tract; thereby, allowing for the transmigration of FD10 from the intestinal lumen into the anterior and caudal capillary venous plexuses (CVP). Micro-angiogram of FD10 via the common cardinal vein (CCV) conferred that UFP exposure disrupted the GVB. In addition, co-gavaging a disintegrin and metalloproteinase domain-containing protein 10 (Adam10) inhibitor to inhibit extracellular proteolysis of Notch receptors mimicked UFP gavage, whereas transient overexpression of Notch signaling via Notch intracellular cytoplasmic domain (NICD) mRNA injection restored UFP-mediated GVB. As a corollary, UFP down-regulated transcription of cytoplasmic zonula occludens1 (ZO1), and the transmembrane claudin 1 (Cldn1), and the Notch target, hairy and enhancer of split-1 (Hes1) in cultured endothelial cells. Overall, the integration of a genetically tractable embryonic zebrafish model with micro-gavage and optical imaging techniques provides the high-throughput screening insights into epigenetic and genetic interaction underlying UFP-mediated disruption of the GVB.

2. Materials and Methods

2.1. Zebrafish Maintenance and Study Approval

All zebrafish experiments were performed in compliance with UCLA Institutional Animal Care and Use Committee (IACUC) protocol (A3196-01; 17 July 2018).

2.2. Collection, Extraction, and Chemical Analysis of Ultrafine Particles (UFP)

Ambient ultrafine particulate matter (UFP particles with aerodynamic diameter $< 0.2 \mu\text{m}$) was collected on PTFE membrane filters ($20 \times 25 \text{ cm}$, $3.0 \mu\text{m}$ pore size, PALL Life Sciences, New York, NY, USA) at the University of Southern California's Particle Instrumentation Unit using a high-volume sampler (with a flow rate of 250 L per minute, lpm) connected to a PM_{2.5} pre-impactor for separation and collection of PM_{2.5}. The loaded filter samples were then extracted in Milli-Q water (Millipore A-10, EMD Millipore, Billerica, MA, USA) following 1 h of sonication, in which the amount of extracted PM_{2.5} via sonication was determined by subtracting the pre-extraction and post-extraction weights of the filters using a high precision ($\pm 0.001 \text{ mg}$) microbalance (MT5, Mettler Toledo Inc., Columbus, OH, USA). Following filter extraction, the highly concentrated aqueous suspensions of PM_{2.5} were diluted to provide the required slurry concentration and stored at $-20 \text{ }^\circ\text{C}$ for experiments. Precise descriptions of sample collection and extraction can be found in Taghvaei et al. [20]. The aqueous suspensions of PM_{2.5} were chemically analyzed for total organic carbon (TOC), water-soluble inorganic ions, and metal elements by Wisconsin State Laboratory of Hygiene. In summary, TOC content of the samples was quantified by means of a Sievers 900 TOC analyzer [21,22]. In addition, ion chromatography was employed to determine water-soluble inorganic ions [23], whereas the metal and trace elements were quantified by inductively-coupled plasma mass spectroscopy analysis [24]. Chemical compositions of UFP are characterized in our previous publication [25].

2.3. Zebrafish Culture, Micro-Injection, and Micro-Gavage Assay

Transgenic Tg(*flk1*: *mCherry*) zebrafish embryos that visualize *mCherry* fluorescence protein under the control of *flk1* (VEGFR2) promoter were harvested from natural mating consisting of a mixture of males and females at the UCLA Zebrafish Core Facility. Embryos were maintained at $28.5 \text{ }^\circ\text{C}$ in fresh standard E3 medium supplemented with 0.05% methylene blue (Sigma Aldrich, MO, USA) and 0.003% phenylthiourea (PTU, Sigma Aldrich, MO, USA) to suppress fungal outbreak and to inhibit melanogenesis. Ectopic overexpression of global Notch signaling pathway was performed by micro-injecting *NICD* mRNA ($10\text{--}20 \text{ pg}\cdot\text{nL}^{-1}$) as previously described [26]. At 2 days post fertilization (dpf), embryos were manually dechorionated for micro-gavage assay [27]. To perform micro-gavage, transgenic Tg(*flk1*: *mCherry*) embryos were immobilized with neutralized tricaine (Sigma Aldrich, MO, USA) and oriented in 1% low melting agarose (ThermoFisher, MA, USA). A solution of FD10 (Sigma Aldrich, MO, USA) containing 0.05% phenol-red dye (Sigma Aldrich, MO, USA) was micro-gavaged into the anterior intestinal bulb without damaging the esophagus, the swim bladder, or the yolk sac (Figure 1D). UFP ($25\text{--}50 \mu\text{g}\cdot\text{mL}^{-1}$), Adam10 inhibitor ($5 \mu\text{M}$, GI254023X, Sigma Aldrich, MO, USA), or ethylenediaminetetraacetic acid (EDTA) (20 mM , Sigma Aldrich, MO, USA) were homogenized in the FD10 solution respectively for micro-gavage. At 7 hpg, distribution of FD10 in the AVP and CVP were imaged with dual channel confocal (Leica SP8, Wetzlar, Germany) or inverted fluorescence microscopy (Olympus, IX70) previously described [25,28].

2.4. Micro-Angiogram via Common Cardinal Vein (CCV)

Immobilized Tg(*flk1*: *mCherry*) embryos were placed on a 3% agar plate to perform the micro-angiography. A mixture of the gavage solution (FD10 solution and 0.05% phenol-red dye) was injected into the zebrafish CCV as previously described [29,30]. Micro-angiogram was verified by imaging FD10 fluorescence in the DA and PCV. At 1 h post injection, injected embryos were embedded

in 1% low melting agarose for fluorescence imaging. Distribution of the FD10 in the AVP and CVP was evaluated under inverted fluorescence microscope (Olympus, IX70).

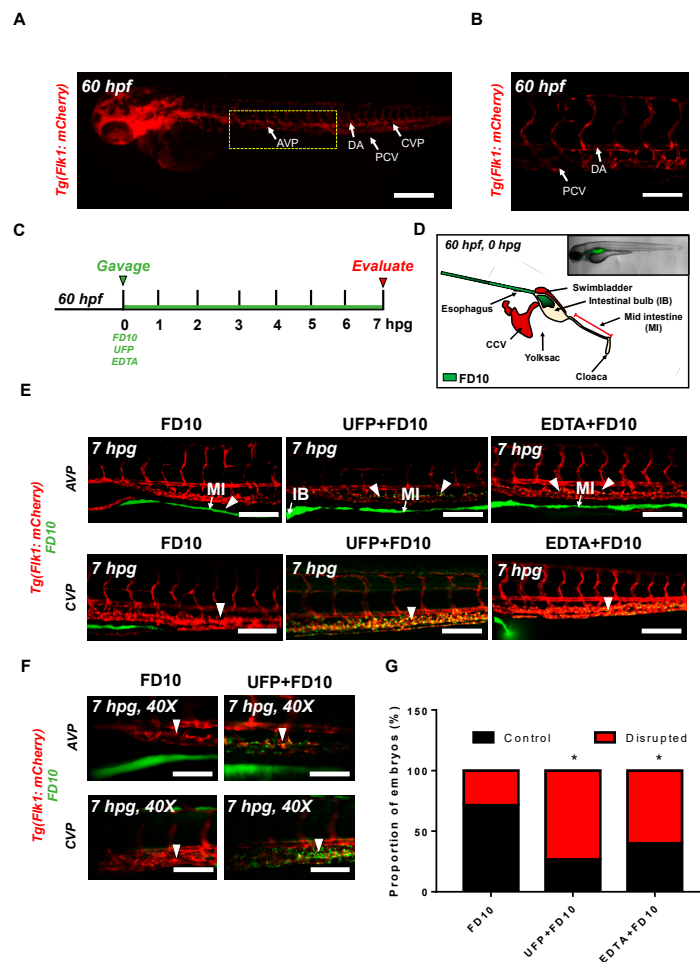


Figure 1. Acute ultrafine particulate matter (UFP) ingestion disrupts intestinal epithelial barrier integrity. Transgenic Tg(*flk1*: mCherry) zebrafish embryos at 60 hpf were micro-gavaged with FITC-conjugated dextran (FD10, 10 kDa). (A,B) Anatomy of endothelial vasculature in the Tg(*flk1*: mCherry) embryo. DA: dorsal aorta; PCV: posterior caudal vein; AVP: anterior venous capillary plexus; CVP: caudal vein capillary plexus; Scale bar: 32 μ m. (C) Experimental design: At 2 dpf, embryos were randomly chosen for micro-gavage with FD10 solution with or without UFP or EDTA at 20 mM. Intestinal barrier integrity and translocation of FD10 to vascular endolumen (*flk1*⁺) were evaluated at 7 h post gavage (hpg). (D) A schematic representation of micro-gavage in an embryonic gastrointestinal (GI) tract. FD10 solution was micro-gavaged in the intestinal bulb without disrupting the esophagus, swim bladder and yolk sac. (E) Representative images of the AVP and CVP at 7 hpg. In FD10 gavaged-controls, FD10 remained only in the intestinal bulb and mid-intestine. In contrast, co-gavaging FD10 with UFP or ethylenediaminetetraacetic acid (EDTA) accumulated FD10 in the AVP and CVP (white arrow heads). Scale bar: 20 μ m. (F) Magnified view of the AVP and CVP. Scale bar: 20 μ m. (G) Percentage of embryos exhibiting endoluminal FD10 fluorescence (* $p < 0.05$ vs. FD10, $n = 10$ per group).

2.5. Human Aortic Endothelial Cell (HAEC) Culture and Quantitative Real-Time Polymerase Chain Reaction (qRT-PCR) Analyses

For qRT-PCR analyses, HAEC (Cell Applications, San Diego, CA, USA) between passages 4 and 10 were maintained on 0.1% bovine gelatin-coated plates (Midsci, St. Louis, MO, USA) at 37 °C and 5% CO₂. EC growth medium (Cell Applications, San Diego, CA, USA) was supplemented with 5% fetal bovine serum (FBS, Life technologies, Carlsbad, CA, USA) and 1% penicillin-streptomycin (P/S,

Carlsbad, CA, USA) to promote cultivation. Confluent HAEC monolayers were exposed to UFP, Adam10 inhibitor, Iwr1 (10 μ M, Sigma Aldrich, St. Louis, MO, USA), or lithium chloride (LiCl, 20 mM) respectively in neutralized M199 media (Life Technologies, Carlsbad, CA, USA). Total RNA was collected following 6 h of treatment. RNA purification and reverse transcription were performed as previously described [28]. qPCR master-mix (Applied Biological Materials Inc., Richmond, BC, Canada) was used for PCR amplification. mRNA levels were assessed and compared by the $\Delta\Delta$ Ct method. mRNA expression was normalized to human actin expression. Sequences of primers are listed in Table 1.

Table 1. Sequencing Information of qRT-PCR primers.

Primers	qRT-PCR Primer Sequence (5'-3')	
Human Actin	Forward	ACCCACACTGTGCCCATCTAC
	Reverse	TCGGTGAGGATCTTCATGAGG
Human Zo1	Forward	CGCCAAGAGCACAGCAATGGA
	Reverse	CCCACTCTGAAAATGAGGATT
Human Cldn1	Forward	GTGACCGCCTTCTGGACCAC
	Reverse	TGCTCAGAGCCAGCACCGAGT
Human Hes1	Forward	TGAGCCAGCTGAAAACACTG
	Reverse	GTGCGCACCTCGGTATTAAC

2.6. Statistics

Data were expressed as mean \pm standard deviation and compared among separate experiments. Unpaired two-tail t test and 2-proportion z-test were performed for statistical comparisons between 2 experimental conditions; p -values < 0.05 were considered significant.

3. Results

3.1. Acute UFP Ingestion Disrupts Intestinal Barrier Integrity and Maturation of GI Tract

To assess whether acute UFP ingestion disrupts the embryonic intestinal barrier, FD10 suspension containing UFP (25 μ g·mL⁻¹) or the positive control EDTA (20 mM) was micro-gavaged to transgenic Tg(flkl1: mCherry) zebrafish embryos at 60 h post fertilization (hpf) (Figure 1A–C). Modulated intestinal permeability and the barrier integrity as denoted by co-localization of FD10 fluorescence and vascular endothelium (flkl1⁺) was evaluated at 7 hpg (Figure 1C, Figure S1). In the FD10-gavaged controls, FD10 remained in the intestinal bulb and mid-intestine, migrating solely through the cloaca. In contrast, co-gavage with UFP perfused intestinal FD10 fluorescence into venous capillary plexus, between the dorsal aorta (DA) and posterior cardinal vein (PCV). Approximately 80% of UFP-gavaged embryos exhibited luminal fluorescence in both AVP and CVP. In addition, co-gavage with EDTA that induced structural deformation of epithelial TJ phenocopied UFP-gavaged embryos ($* p < 0.05$ vs. FD10, $n = 10$ per each group) (Figure 1E–G). We further examined whether acute UFP ingestion regulates villus ultrastructure in the embryonic GI tract. At 7 hpg, the distribution of intestinal FD10 fluorescence was assessed to confer the morphology of the mid-intestine (Figure 2A). While luminal FD10 fluorescence in mid-intestine was prominent in FD10-gavaged controls, co-gavage with UFP systemically reduced intestinal FD10 fluorescence in 80% of gavaged embryos ($* p < 0.05$ vs. FD10, $n = 10$ per each group) (Figure 2B–D). Thus, our data suggest that acute UFP ingestion via micro-gavage disrupts the intestinal barrier integrity and retards maturation of the embryonic GI system.

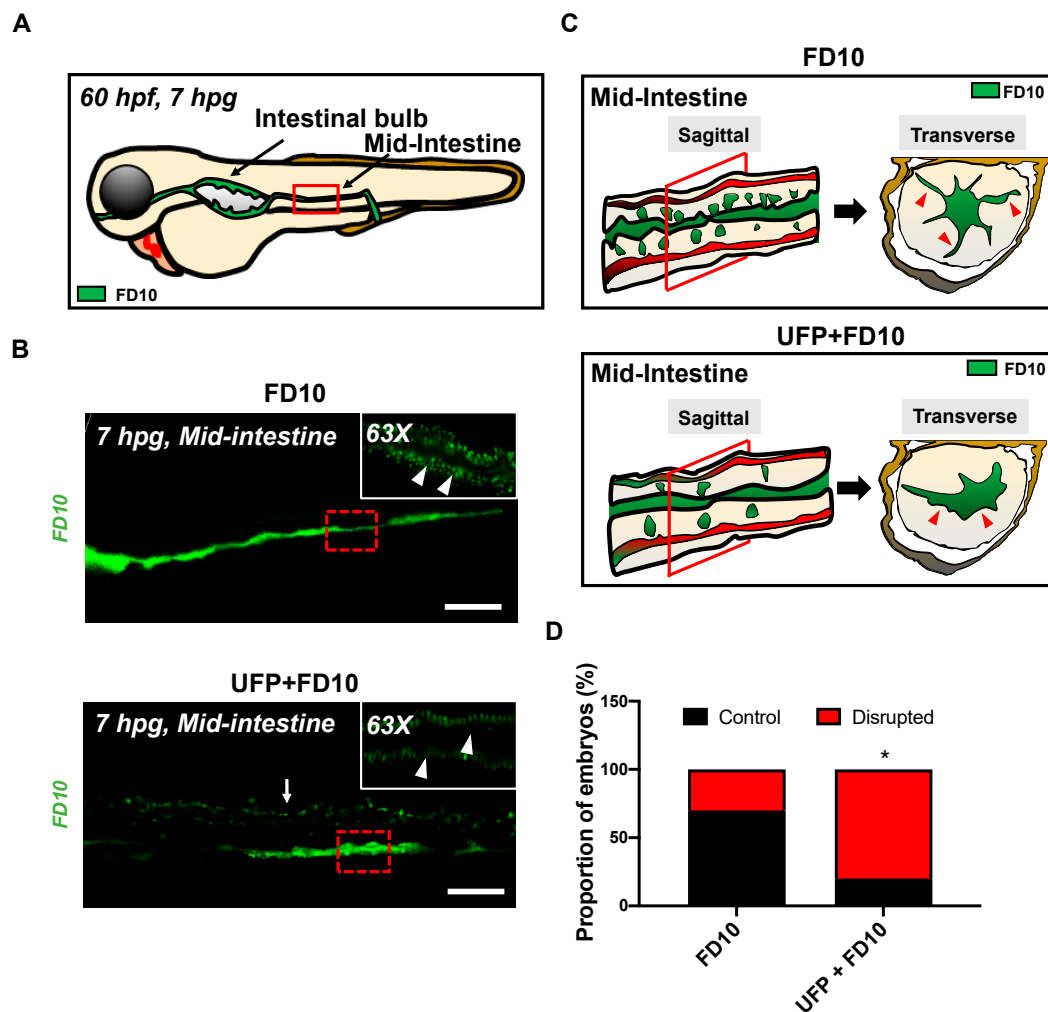


Figure 2. Acute UFP exposure disrupts maturation of embryonic GI tract. (A) Schematic representation of the embryonic GI tract at 7 hpg. The density of FD10 fluorescence in the mid-intestine was assessed to evaluate maturation of the GI tract (Red box). (B) Representative images of UFP-disrupted GI tract (white dashed box). Compared to FD10-gavaged controls, co-gavaging UFP, as denoted with endoluminal FD10 fluorescence (white arrow), altered morphology and systemically reduced the density of FD10 fluorescence in the mid-intestine (white arrowheads, $n = 5$ per group). Scale bar: 20 μm . (C) Schematic representations of sagittal and transverse views of the mid-intestine with and without UFP gavage. Acute UFP exposure in developing GI system retards maturation (red arrowheads). (D) Percentage of embryos exhibiting reduced FD10 density in the mid intestine (* $p < 0.05$ vs. FD10, $n = 10$ per group).

3.2. Micro-Angiography via CCV to Mimic UFP Gavage

The UFP-disrupted intestinal barrier is further supported by performing micro-angiography in the zebrafish micro-circulation system (Figure 3A). Immediately following micro-angiography, the micro-circulatory system in transgenic Tg(flk1: mCherry) embryos, including the injection site, CCV, heart, the DA and PCV, exhibited prominent FD10 fluorescence (Figure 3B). At 1 h post injection (hpi), FD10 fluorescence was observed in both AVP and CVP mimicking UFP gavage ($n = 5$) (Figure 3C,D). Thus, our micro-angiography results suggested the notion that UFP gavage impaired endothelial microenvironment via disrupted intestinal barrier.

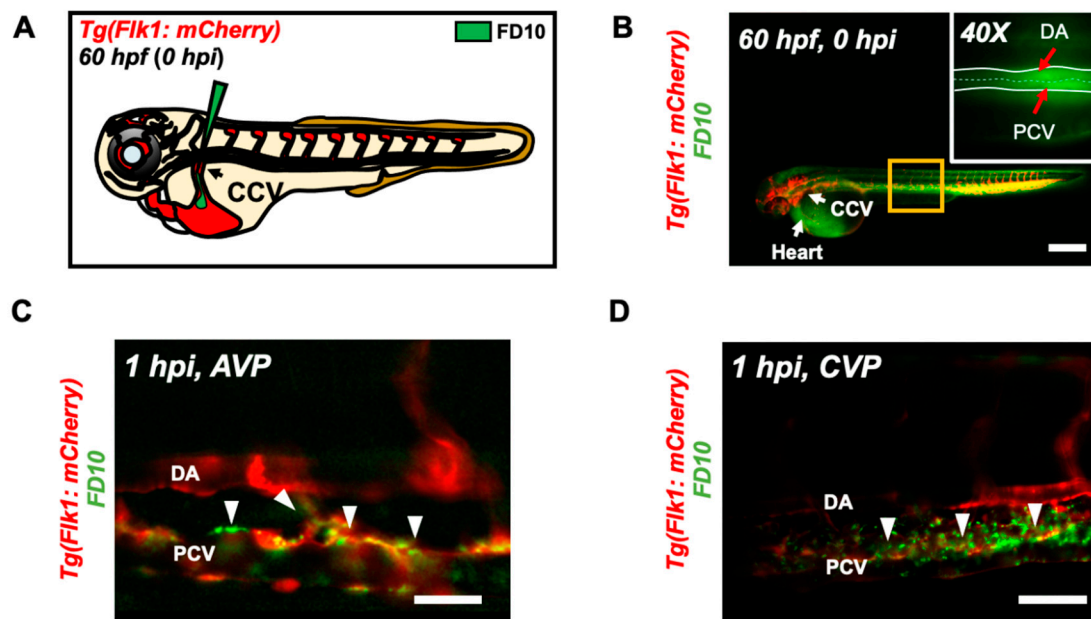


Figure 3. Micro-angiography via common cardinal vein (CCV) to mimic UFP gavage. (A) A schematic representation of micro-angiography via CCV to introduce FD10 to the microcirculatory system. (B) A representative image of the transgenic Tg(flk1: mCherry) embryo following FD10 injection to CCV. At 0 hpi, FD10 fluorescence was prominent at the injection site, CCV, heart, DA and PCV. Scale bar: 100 μm . (C,D) At 1 hpi, FD10 was distributed in the AVP and CVP, between the DA and PCV, mimicking UFP gavage-mediated effects (white arrowheads, $n = 5$ per group). Scale bar: 32 μm .

3.3. UFP Exposure Regulates Notch-Mediated Endothelial TJ Expression

To corroborate UFP-disrupted intestinal barrier, we assessed the transcription of endothelial TJ, including Zo1, Cldn1, and Ocln1 in cultured HAEC. Exposure to UFP decreased Zo1 and Cldn1 mRNA expression by 23% and 34%, respectively, whereas Ocln1 mRNA expression remained unchanged ($* p < 0.05$ vs. H_2O , $n = 3$). Treatment with the small molecular inhibitor Iwr1, to down-regulate Wnt-mediated TJ expression, reduced Zo1 mRNA by 37% and significantly inhibited Cldn1 and Ocln1 mRNA expression by 83% and 71%, respectively, whereas treatment with lithium chloride (LiCl) for ectopic activation of Wnt/ β -catenin signaling pathway and prevent loss of TJ upregulated both Cldn1 and Ocln1 mRNA expression by 3.1-fold and 2.8-fold ($* p < 0.05$ vs. DMSO for Iwr1, and vs. H_2O for LiCl, $n = 3$) (Figure 4A) [31,32]. As a corollary, UFP exposure led to a dose-dependent reduction in Zo1 and Cldn1 mRNA expression. UFP at $50 \mu\text{g}\cdot\text{mL}^{-1}$ (UFP50) attenuated Zo1 and Cldn1 mRNA expression by 22% and 12%, respectively, as compared to UFP at $25 \mu\text{g}\cdot\text{mL}^{-1}$ (UFP25) ($* p < 0.05$ vs. H_2O , $n = 3$). Similarly, Hes1 mRNA, a Notch target gene, was also reduced in dose-dependent manner (Figure 4B). Treatment of Adam10 inhibitor to suppress global Notch receptor activation down regulated both Cldn1 and Hes1 mRNA expression by 22% and 69%, respectively, as compared to the untreated controls ($* p < 0.05$ vs. DMSO, $n = 3$) (Figure 4C). This finding suggested Notch activity implicates UFP-mediated Cldn1 mRNA expression. Co-gavaging Adam10 inhibitor in zebrafish embryos mimicked UFP gavage by developing luminal FD10 fluorescence in both AVP and CVP. As a corollary, global overexpression of NICD mRNA via micro-injection restored UFP-disrupted intestinal barrier ($* p < 0.05$ vs. FD10, $n = 10$ per group) (Figure 4D,E). Taken together, our data recapitulated UFP exposure modulates TJ expressions in Notch-dependent manner in association with impaired development of the GVB.

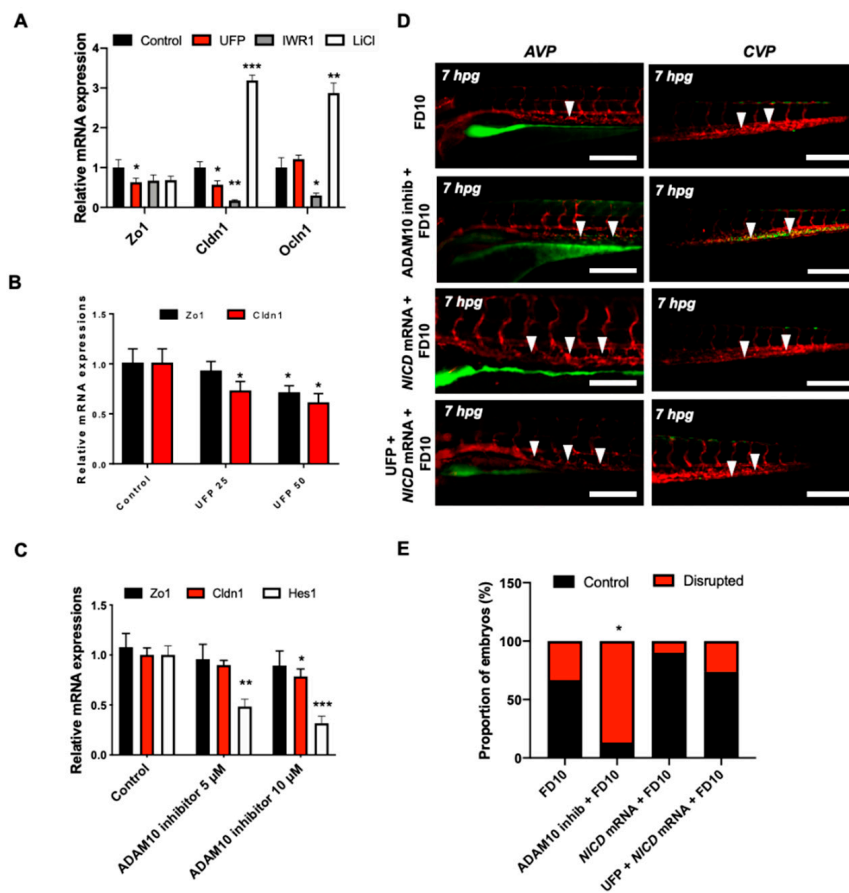


Figure 4. UFP exposure down-regulates mRNA expressions of endothelial tight junction (TJ) protein and the Notch target gene to disrupt the GVB. mRNA expressions of TJ proteins, including zonula occludens1 (Zo1), claudin 1 (Cldn1), and occludin 1 (Ocln1), and the Notch target genes, including Hairy and enhancer of split-1 (Hes1), were assessed in vitro by cultured human aortic endothelial cells (HAEC). (A) UFP exposure (25 $\mu\text{g}\cdot\text{mL}^{-1}$ for 6 h) inhibited Zo1 and Cldn1 mRNA expressions, whereas Ocln1 mRNA remained unchanged. While Iwr1 treatment (10 μM) diminished overall TJ mRNA expression, LiCl (20 mM) up-regulated Cldn1 and Ocln1 mRNA expression (* $p < 0.05$ vs. DMSO for Iwr1, H₂O for LiCl, $n = 3$, ** $p < 0.01$, *** $p < 0.001$). (B) UFP exposure (25–50 $\mu\text{g}\cdot\text{mL}^{-1}$ for 6 h) down-regulated both TJ (Zo1 and Cldn1 mRNA) and Notch target genes (Hes1) mRNA expression in a dose-dependent manner (* $p < 0.05$ vs. H₂O, $n = 3$). (C) Treatment of Adam10 inhibitor (5 μM) to inhibit Notch receptor activation down-regulated Cldn1, and Hes1 mRNA in a dose-dependent manner (* $p < 0.05$ vs. DMSO, $n = 3$, ** $p < 0.01$, *** $p < 0.001$) (D) Micro-gavage with Adam10 inhibitor promoted transmigration of FD10 to both AVP and CVP. Micro-injection of NICD mRNA restored UFP- and Adam10 inhibitor-mediated effect. (E) Percentage of embryos exhibiting endoluminal FD10 fluorescence (* $p < 0.05$ vs. FD10, $n = 10$ per group).

4. Discussion

The novel contribution of our study is to elucidate UFP-disrupted intestinal barrier integrity using the zebrafish system. Utilization of zebrafish embryos provided a high-throughput screening of altering gut-vascular permeability. Micro-gavage of ambient UFP to the transgenic zebrafish embryos promoted transmigration of FD10 from the intestinal epi-lumen to vascular endo-lumen (Figure 1). UFP exposure further led to an impaired embryonic villus ultrastructure during development (Figure 2). Micro-gavage of Adam 10 inhibitor disrupted GVB, whereas micro-injection of NICD mRNA rescued UFP-disrupted intestinal barrier. As a corollary, UFP exposure down-regulated Notch-mediated TJ mRNA expression in cultured HAEC (Figure 4). Overall, UFP exposure down-regulates Notch

signaling-mediated TJ expression to increase endothelial permeability, and subsequently disrupted the GVB (Figure 5).

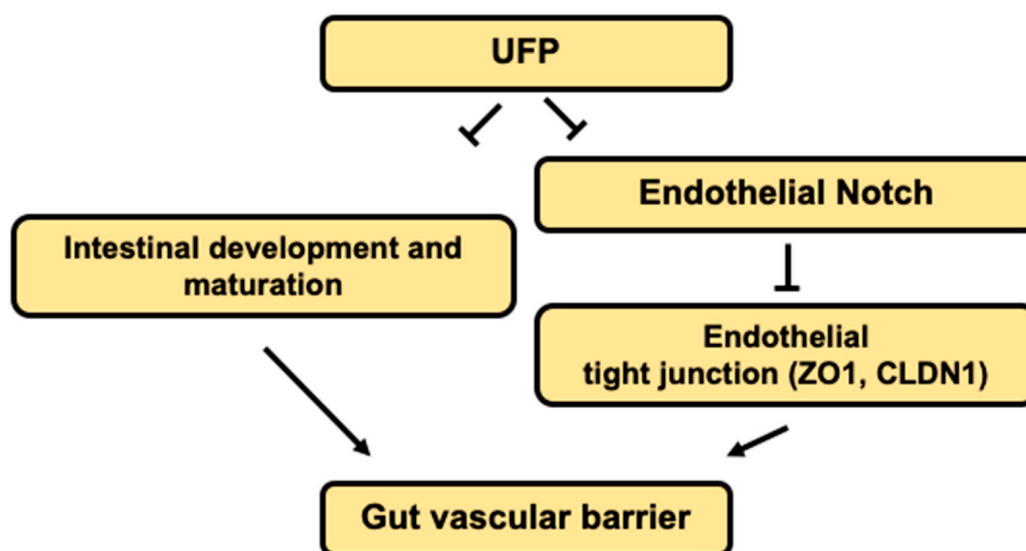


Figure 5. Schematic overviews of the proposed mechanisms.

Ambient UFP are the redox-active sub-fraction of PM_{2.5}, harboring elemental and polycyclic aromatic hydrocarbons emitted from primary diesel combustion and photochemical formation from urban environmental gases [10]. Their small size and large surface-to-volume ratio facilitates potential adsorption in the cardiopulmonary and vascular system associated with pathophysiology of systemic inflammatory responses [33–35]. Increasing epidemiological studies correlate UFP exposure with clinical relevance to intestinal disease and gut microenvironment. Inhaled or dietary UFP ingestion aggravates intestinal dysbiosis and macrophage infiltrates in the GI tract, suggesting altered intestinal barrier [10,17,36]. The venous capillary plexus in the transgenic zebrafish embryos demonstrated prominence in FITC fluorescence following UFP micro-gavage and phenocopied EDTA-dependent barrier disruption (Figure 1). FITC micro-angiogram further mimicked UFP micro-gavage suggesting disrupted embryonic intestinal barrier integrity by increasing endothelial permeability [37]. Herein, our integration of an embryonic zebrafish model with micro-gavage technique provides molecular insights into UFP exposure to disrupt the gut-vascular homeostasis.

Notch signaling is well-recognized as a conserved mechanism for GI epi- and endothelial homeostasis [37–39]. In developing gut, Notch signaling involves multi-potential stem/progenitor cell proliferation and lineage [40]. Inhibition of global Notch activity, including pharmacological inhibition, genetic recombination, and neutralizing antibodies, leads to an overall reduction in gastric epithelial and intestinal stem cell proliferation, whereas overexpression of NICD to increase systemic Notch activity promotes the proliferation of gastric stem cells [41–45]. Moreover, intestinal Notch activation via Delta D programs the differentiation of absorptive enterocytes [40]. While reduction in Notch activity results in secretory cell hyperplasia, constitutively-active NICD shifts the differentiation of secretory cells [40,46]. The interplay between Wnt and Notch is also recognized to direct the fate of intestinal epithelial cells [47]. In the transgenic zebrafish model of UFP micro-gavage, we observed an alteration of FITC fluorescence pattern and intestinal ultrastructure (Figure 3). Hence, UFP exposure at the early stage of the development could systemically reprogram intestinal cell fate and interfere proliferation for immature intestinal maturation.

Dysregulation of the Notch ligand Delta-like ligand 4 (Dll4), or Notch 1 receptor expression, induces hyper-permeability and transcytosis in murine retina, while down-regulation of Notch 4 expression is associated with endothelial blood–brain barrier dysfunction [48,49]. The role of Notch activity in vascular stabilization and cell quiescence is also well-recognized [39]. In parallel, differential

patterning of VE-cadherin in the absence of Notch activity supports the regulatory effects of junctional stability [50]. Consistent with the current literature, UFP exposure concurrently down-regulated Hes1 and Cldn1 mRNA expression in dose-dependent manner, suggesting increased endothelial permeability (Figure 4B). Thus, our data supports that UFP ingestion inhibits Notch-mediated intestinal barrier integrity by modulating the level of endothelial TJ expressions (see the proposed mechanism in Figure 5).

While transient genetic manipulations are robust and concise methods to modulate global expression, utilization of tissue-specific mutant strain is crucial. Advanced genomic engineering methods paved a new way for conditional tissue-specific knockdown strategies. A growing body of evidence, however, indicated retarded embryogenesis and increased embryonic lethality in the absence of Notch signaling pathway. Homozygous deficiency in the Notch ligand, Jagged1, results in defective vascular remodeling and elevate risk of embryonic lethality [51]. Haploinsufficiency in delta-like ligand 4 further retards gross morphology and arteriogenesis to promote embryonic lethality [52]. Therefore, the strategy of generating a mutant strain should be carefully designed for follow up studies.

Whether and how UFP ingestion mitigates intestinal Notch activity remains as an unexplored question. The transcription factor Forkhead box sub-family O1 (FOXO1) enhances repressor clearance and forms a transcriptional activation complex during Notch activation [25,53]. In colonic tumorous tissue, ectopic level of FOXO1 expression alters epithelial permeability, villus ultrastructure, and arrangements in the GI tract [54]. Furthermore, intestinal epithelial FOXO1 expression associates GI barrier integrity [55,56]. At the molecular level, concurrent nuclear retention of FOXO1 and β -catenin represses Cldn5 expression in the cerebral vascular endothelium [57]. While ambient PM exposure epigenetically controls of cardiometabolic state, endothelial FOXO1 couples cellular metabolism and endothelial homeostasis [58]. Our previous report indicates UFP exposure-mediated cytoplasmic FOXO1 expressions in vascular endothelial cells [25]. Whether UFP-decreased intestinal FOXO1 expression participates in Notch-mediated GVB warrants further investigation.

Our data draw the line from UFP exposure to intestinal barrier disruption through Notch signaling. However, the GVB is regulated by multiple signaling mechanisms that are linked or plays parallel roles. UFP and consequent chronic inflammation has been widely recognized to increase reactive oxygen species and vascular oxidative stress [59]. While UFP increases the level of Jun N-terminal kinase (JNK) activation, pharmacological JNK inhibition restores UFP-inhibited vascular endothelial Notch signaling pathway in vitro [25,59]. Thus, oxidative stress-related pathways such as JNK signaling could underly UFP-disrupted GVB. Moreover, exposure to ambient particular matter has been reported to induce global alteration of microRNA (miR) profiles in various organs. For instance, PM rich in transition metal components increase miR-222 and miR-21 in peripheral blood leukocytes [60]. miR-1, -9, -135a and -222 are associated with PM exposure, whereas miR-223 and -375 has been systemically regulate airway inflammation [61–63]. Therefore, miRs may also play a pivotal role in regulating the barrier integrity following UFP ingestion.

Three-dimensional (3D) imaging techniques to visualize intestinal ultrastructure remain a challenge due to constant intestinal peristalsis and gut motility, necessitating a robust imaging technique with high spatiotemporal resolution and rapid data acquisition. The advent of light-sheet fluorescence microscopy (LSFM) allows for real-time imaging of the peristaltic contraction and the ultrastructure of the GI tract [64–66]. The integration of LSFM with zebrafish genetics and deep learning for post-imaging processing enables precise time-lapse monitoring of myocardial contraction and intracardiac flow dynamics [67]. Thus, interfacing LSFM with the transgenic zebrafish system and micro-gavage technique may allow for time-lapse assessment of FITC distribution and varying intestinal architecture and barrier disruption in 3D, providing a new imaging insight into biomedical and environmental health research.

Overall, we demonstrate a zebrafish model for rapid screening of GVB in response to epigenetic stimuli. We demonstrate new molecular insights into UFP-mediated Notch signaling to disrupt GVB.

Supplementary Materials: The following are available online at <http://www.mdpi.com/2305-6304/8/4/107/s1>. Figure S1. Imaging endoluminal distribution of FD10.

Author Contributions: Conceptualization, K.I.B. and T.K.H.; methodology, K.I.B. and Y.Q.; software, K.I.B. and C.-C.C.; validation, C.-C.C. and R.O.; formal analysis, K.I.B.; investigation, K.I.B.; resources, E.S., C.S. and T.K.H.; writing—original draft preparation, K.I.B. And Y.Q.; writing—review and editing, R.L., T.K.H. and R.O.; visualization, K.I.B. and C.-C.C.; supervision, R.L., T.K.H.; project administration, T.K.H.; funding acquisition, T.K.H. All authors have read and agreed to the published version of the manuscript.

Funding: This study was supported by National Institutes of Health R01HL083015 (TKH), R01HL111437 (TKH), R01HL129727 (TKH), R01HL118650 (TKH), I01 BX004356 (TKH).

Acknowledgments: The authors like to express their gratitude to Weinmaster for providing the NICD plasmid, and Yuan Dong at UCLA zebrafish core facility for generously providing Tg(flk1:mCherry) zebrafish line.

Conflicts of Interest: The authors declare no conflict of interest.

References

- Nel, A.; Xia, T.; Madler, L.; Li, N. Toxic potential of materials at the nanolevel. *Science* **2006**, *311*, 622–627. [[CrossRef](#)] [[PubMed](#)]
- Zhang, Y.; Schauer, J.J.; Shafer, M.M.; Hannigan, M.P.; Dutton, S.J. Source apportionment of in vitro reactive oxygen species bioassay activity from atmospheric particulate matter. *Environ. Sci. Technol.* **2008**, *42*, 7502–7509. [[CrossRef](#)] [[PubMed](#)]
- Kaplan, G. Air pollution and the inflammatory bowel diseases. *Inflamm. Bowel Dis.* **2011**, *17*, 1146–1148. [[CrossRef](#)] [[PubMed](#)]
- Beamish, L.A.; Osornio-Vargas, A.R.; Wine, E. Air pollution: An environmental factor contributing to intestinal disease. *J. Crohns Colitis* **2011**, *5*, 279–286. [[CrossRef](#)] [[PubMed](#)]
- Lomer, M.C.; Thompson, R.P.; Powell, J.J. Fine and ultrafine particles of the diet: Influence on the mucosal immune response and association with Crohn's disease. *Proc. Nutr. Soc.* **2002**, *61*, 123–130. [[CrossRef](#)] [[PubMed](#)]
- Moller, W.; Haussinger, K.; Winkler-Heil, R.; Stahlhofen, W.; Meyer, T.; Hofmann, W.; Heyder, J. Mucociliary and long-term particle clearance in the airways of healthy nonsmoker subjects. *J. Appl. Physiol.* **2004**, *97*, 2200–2206. [[CrossRef](#)]
- Moller, W.; Haussinger, K.; Ziegler-Heitbrock, L.; Heyder, J. Mucociliary and long-term particle clearance in airways of patients with immotile cilia. *Respir. Res.* **2006**, *7*, 10. [[CrossRef](#)]
- Weir, A.; Westerhoff, P.; Fabricius, L.; Hristovski, K.; von Goetz, N. Titanium dioxide nanoparticles in food and personal care products. *Environ. Sci. Technol.* **2012**, *46*, 2242–2250. [[CrossRef](#)]
- Li, R.; Ning, Z.; Majumdar, R.; Cui, J.; Takabe, W.; Jen, N.; Sioutas, C.; Hsiai, T. Ultrafine particles from diesel vehicle emissions at different driving cycles induce differential vascular pro-inflammatory responses: Implication of chemical components and NF-kappaB signaling. *Part. Fibre Toxicol.* **2010**, *7*, 6. [[CrossRef](#)]
- Li, R.; Navab, K.; Hough, G.; Daher, N.; Zhang, M.; Mittelstein, D.; Lee, K.; Pakbin, P.; Saffari, A.; Bhetraratana, M.; et al. Effect of exposure to atmospheric ultrafine particles on production of free fatty acids and lipid metabolites in the mouse small intestine. *Environ. Health Perspect.* **2015**, *123*, 34–41. [[CrossRef](#)]
- Shen, W.; Gaskins, H.R.; McIntosh, M.K. Influence of dietary fat on intestinal microbes, inflammation, barrier function and metabolic outcomes. *J. Nutr. Biochem.* **2014**, *25*, 270–280. [[CrossRef](#)] [[PubMed](#)]
- Turner, J.R. Intestinal mucosal barrier function in health and disease. *Nat. Rev. Immunol.* **2009**, *9*, 799–809. [[CrossRef](#)] [[PubMed](#)]
- Bouziat, R.; Jabri, B. IMMUNOLOGY. Breaching the gut-vascular barrier. *Science* **2015**, *350*, 742–743. [[CrossRef](#)] [[PubMed](#)]
- Spadoni, I.; Zagato, E.; Bertocchi, A.; Paolinelli, R.; Hot, E.; Di Sabatino, A.; Caprioli, F.; Bottiglieri, L.; Oldani, A.; Viale, G.; et al. A gut-vascular barrier controls the systemic dissemination of bacteria. *Science* **2015**, *350*, 830–834. [[CrossRef](#)]
- Tuma, P.; Hubbard, A.L. Transcytosis: Crossing cellular barriers. *Physiol. Rev.* **2003**, *83*, 871–932. [[CrossRef](#)]
- Wu, G.D. The Gut Microbiome, Its Metabolome, and Their Relationship to Health and Disease. *Nestle Nutr. Inst. Workshop Ser.* **2016**, *84*, 103–110. [[CrossRef](#)]

17. Li, R.; Yang, J.; Saffari, A.; Jacobs, J.; Baek, K.I.; Hough, G.; Larauche, M.H.; Ma, J.; Jen, N.; Moussaoui, N.; et al. Ambient Ultrafine Particle Ingestion Alters Gut Microbiota in Association with Increased Atherogenic Lipid Metabolites. *Sci. Rep.* **2017**, *7*, 42906. [[CrossRef](#)]
18. Mutlu, E.A.; Engen, P.A.; Soberanes, S.; Urich, D.; Forsyth, C.B.; Nigdelioglu, R.; Chiarella, S.E.; Radigan, K.A.; Gonzalez, A.; Jakate, S.; et al. Particulate matter air pollution causes oxidant-mediated increase in gut permeability in mice. *Part. Fibre Toxicol.* **2011**, *8*, 19. [[CrossRef](#)]
19. Kumar, S.; Hedges, S.B. A molecular timescale for vertebrate evolution. *Nature* **1998**, *392*, 917–920. [[CrossRef](#)]
20. Taghvaei, S.; Mousavi, A.; Sowlat, M.H.; Sioutas, C. Development of a novel aerosol generation system for conducting inhalation exposures to ambient particulate matter (PM). *Sci. Total Environ.* **2019**, *665*, 1035–1045. [[CrossRef](#)]
21. Kristensen, T.B.; Du, L.; Nguyen, Q.T.; Nøjgaard, J.K.; Koch, C.B.; Nielsen, O.F.; Hallar, A.G.; Lowenthal, D.H.; Nekat, B.; Van Pinxteren, D.; et al. Chemical properties of HULIS from three different environments. *J. Atmos. Chem.* **2015**, *72*, 65–80. [[CrossRef](#)]
22. Stone, E.A.; Snyder, D.C.; Sheesley, R.J.; Sullivan, A.P.; Weber, R.J.; Schauer, J.J. Source apportionment of fine organic aerosol in Mexico City during the MILAGRO experiment 2006. *Atmos. Chem. Phys.* **2008**, *8*, 1249–1259. [[CrossRef](#)]
23. Lough, G.C.; Schauer, J.J.; Park, J.S.; Shafer, M.M.; Deminter, J.T.; Weinstein, J.P. Emissions of metals associated with motor vehicle roadways. *Environ. Sci. Technol.* **2005**, *39*, 826–836. [[CrossRef](#)] [[PubMed](#)]
24. Herner, J.D.; Green, P.G.; Kleeman, M.J. Measuring the trace elemental composition of size-resolved airborne particles. *Environ. Sci. Technol.* **2006**, *40*, 1925–1933. [[CrossRef](#)] [[PubMed](#)]
25. Baek, K.I.; Packard, R.R.S.; Hsu, J.J.; Saffari, A.; Ma, Z.; Luu, A.P.; Pietersen, A.; Yen, H.; Ren, B.; Ding, Y.; et al. Ultrafine Particle Exposure Reveals the Importance of FOXO1/Notch Activation Complex for Vascular Regeneration. *Antioxid. Redox Signal.* **2018**, *28*, 1209–1223. [[CrossRef](#)] [[PubMed](#)]
26. Lee, J.; Vedula, V.; Baek, K.I.; Chen, J.; Hsu, J.J.; Ding, Y.; Chang, C.C.; Kang, H.; Small, A.; Fei, P.; et al. Spatial and temporal variations in hemodynamic forces initiate cardiac trabeculation. *JCI Insight* **2018**, *3*. [[CrossRef](#)]
27. Cocchiari, J.L.; Rawls, J.F. Microgavage of zebrafish larvae. *J. Vis. Exp.* **2013**. [[CrossRef](#)]
28. Baek, K.I.; Li, R.; Jen, N.; Choi, H.; Kaboodrangi, A.; Ping, P.; Liem, D.; Beebe, T.; Hsiai, T.K. Flow-Responsive Vascular Endothelial Growth Factor Receptor-Protein Kinase C Isoform Epsilon Signaling Mediates Glycolytic Metabolites for Vascular Repair. *Antioxid. Redox Signal.* **2018**, *28*, 31–43. [[CrossRef](#)]
29. Cianciolo Cosentino, C.; Roman, B.L.; Drummond, I.A.; Hukriede, N.A. Intravenous microinjections of zebrafish larvae to study acute kidney injury. *J. Vis. Exp.* **2010**. [[CrossRef](#)]
30. In Baek, K.; Chang, S.-S.; Chang, C.-C.; Roustei, M.; Ding, Y.; Wang, Y.; Chen, J.; O'donnelle, R.; Chen, H.; Ashby, J.W.; et al. Vascular Injury Changes Topology of Vessel Network to Adapt to Partition of Blood Flow for New Arteriovenous Specification. *bioRxiv* **2020**. [[CrossRef](#)]
31. Li, R.; Beebe, T.; Jen, N.; Yu, F.; Takabe, W.; Harrison, M.; Cao, H.; Lee, J.; Yang, H.; Han, P.; et al. Shear stress-activated Wnt-angiopoietin-2 signaling recapitulates vascular repair in zebrafish embryos. *Arterioscler. Thromb. Vasc. Biol.* **2014**, *34*, 2268–2275. [[CrossRef](#)] [[PubMed](#)]
32. He, Z.; Zhou, Y.; Wang, Q.; Li, J.; Zheng, Z.; Chen, J.; Zhang, H.; Wang, Z.; Xu, H.; Xiao, J. Inhibiting endoplasmic reticulum stress by lithium chloride contributes to the integrity of blood-spinal cord barrier and functional recovery after spinal cord injury. *Am. J. Transl. Res.* **2017**, *9*, 1012–1024. [[PubMed](#)]
33. Schulz, H.; Harder, V.; Ibal-Mulli, A.; Khandoga, A.; Koenig, W.; Krombach, F.; Radykewicz, R.; Stampfl, A.; Thorand, B.; Peters, A. Cardiovascular effects of fine and ultrafine particles. *J. Aerosol. Med.* **2005**, *18*, 1–22. [[CrossRef](#)] [[PubMed](#)]
34. Frampton, M.W. Systemic and cardiovascular effects of airway injury and inflammation: Ultrafine particle exposure in humans. *Environ. Health Perspect.* **2001**, *109* (Suppl. 4), 529–532. [[CrossRef](#)] [[PubMed](#)]
35. Nemmar, A.; Hoet, P.H.; Vanquickenborne, B.; Dinsdale, D.; Thomeer, M.; Hoylaerts, M.F.; Vanbilloen, H.; Mortelmans, L.; Nemery, B. Passage of inhaled particles into the blood circulation in humans. *Circulation* **2002**, *105*, 411–414. [[CrossRef](#)]
36. Salim, S.Y.; Kaplan, G.G.; Madsen, K.L. Air pollution effects on the gut microbiota: A link between exposure and inflammatory disease. *Gut Microbes* **2014**, *5*, 215–219. [[CrossRef](#)]
37. Li, R.; Ning, Z.; Cui, J.; Yu, F.; Sioutas, C.; Hsiai, T. Diesel exhaust particles modulate vascular endothelial cell permeability: Implication of ZO-1 expression. *Toxicol. Lett.* **2010**, *197*, 163–168. [[CrossRef](#)]

38. Demitrack, E.S.; Samuelson, L.C. Notch regulation of gastrointestinal stem cells. *J. Physiol.* **2016**, *594*, 4791–4803. [[CrossRef](#)]
39. Mack, J.J.; Iruela-Arispe, M.L. NOTCH regulation of the endothelial cell phenotype. *Curr. Opin. Hematol.* **2018**, *25*, 212–218. [[CrossRef](#)]
40. Fre, S.; Huyghe, M.; Mourikis, P.; Robine, S.; Louvard, D.; Artavanis-Tsakonas, S. Notch signals control the fate of immature progenitor cells in the intestine. *Nature* **2005**, *435*, 964–968. [[CrossRef](#)]
41. Riccio, O.; van Gijn, M.E.; Bezdek, A.C.; Pellegrinet, L.; van Es, J.H.; Zimmer-Strobl, U.; Strobl, L.J.; Honjo, T.; Clevers, H.; Radtke, F. Loss of intestinal crypt progenitor cells owing to inactivation of both Notch1 and Notch2 is accompanied by derepression of CDK inhibitors p27Kip1 and p57Kip2. *EMBO Rep.* **2008**, *9*, 377–383. [[CrossRef](#)] [[PubMed](#)]
42. Wu, Y.; Cain-Hom, C.; Choy, L.; Hagenbeek, T.J.; de Leon, G.P.; Chen, Y.; Finkle, D.; Venook, R.; Wu, X.; Ridgway, J.; et al. Therapeutic antibody targeting of individual Notch receptors. *Nature* **2010**, *464*, 1052–1057. [[CrossRef](#)]
43. Tran, I.T.; Sandy, A.R.; Carulli, A.J.; Ebens, C.; Chung, J.; Shan, G.T.; Radojicic, V.; Friedman, A.; Gridley, T.; Shelton, A.; et al. Blockade of individual Notch ligands and receptors controls graft-versus-host disease. *J. Clin. Investig.* **2013**, *123*, 1590–1604. [[CrossRef](#)] [[PubMed](#)]
44. Carulli, A.J.; Keeley, T.M.; Demitrack, E.S.; Chung, J.; Maillard, I.; Samuelson, L.C. Notch receptor regulation of intestinal stem cell homeostasis and crypt regeneration. *Dev. Biol.* **2015**, *402*, 98–108. [[CrossRef](#)] [[PubMed](#)]
45. Demitrack, E.S.; Gifford, G.B.; Keeley, T.M.; Carulli, A.J.; VanDussen, K.L.; Thomas, D.; Giordano, T.J.; Liu, Z.; Kopan, R.; Samuelson, L.C. Notch signaling regulates gastric antral LGR5 stem cell function. *EMBO J.* **2015**, *34*, 2522–2536. [[CrossRef](#)] [[PubMed](#)]
46. Crosnier, C.; Vargesson, N.; Gschmeissner, S.; Ariza-McNaughton, L.; Morrison, A.; Lewis, J. Delta-Notch signalling controls commitment to a secretory fate in the zebrafish intestine. *Development* **2005**, *132*, 1093–1104. [[CrossRef](#)]
47. Nakamura, T.; Tsuchiya, K.; Watanabe, M. Crosstalk between Wnt and Notch signaling in intestinal epithelial cell fate decision. *J. Gastroenterol.* **2007**, *42*, 705–710. [[CrossRef](#)] [[PubMed](#)]
48. Yang, J.M.; Park, C.S.; Kim, S.H.; Noh, T.W.; Kim, J.H.; Park, S.; Lee, J.; Park, J.R.; Yoo, D.; Jung, H.H.; et al. Dll4 Suppresses Transcytosis for Arterial Blood-Retinal Barrier Homeostasis. *Circ. Res.* **2020**, *126*, 767–783. [[CrossRef](#)] [[PubMed](#)]
49. Manda, V.K.; Mittapalli, R.K.; Geldenhuys, W.J.; Lockman, P.R. Chronic exposure to nicotine and saquinavir decreases endothelial Notch-4 expression and disrupts blood-brain barrier integrity. *J. Neurochem.* **2010**, *115*, 515–525. [[CrossRef](#)]
50. Bentley, K.; Franco, C.A.; Philippides, A.; Blanco, R.; Dierkes, M.; Gebala, V.; Stanchi, F.; Jones, M.; Aspalter, I.M.; Cagna, G.; et al. The role of differential VE-cadherin dynamics in cell rearrangement during angiogenesis. *Nat. Cell Biol.* **2014**, *16*, 309–321. [[CrossRef](#)]
51. Xue, Y.; Gao, X.; Lindsell, C.E.; Norton, C.R.; Chang, B.; Hicks, C.; Gendron-Maguire, M.; Rand, E.B.; Weinmaster, G.; Gridley, T. Embryonic lethality and vascular defects in mice lacking the Notch ligand Jagged1. *Hum. Mol. Genet.* **1999**, *8*, 723–730. [[CrossRef](#)] [[PubMed](#)]
52. Gale, N.W.; Dominguez, M.G.; Noguera, I.; Pan, L.; Hughes, V.; Valenzuela, D.M.; Murphy, A.J.; Adams, N.C.; Lin, H.C.; Holash, J.; et al. Haploinsufficiency of delta-like 4 ligand results in embryonic lethality due to major defects in arterial and vascular development. *Proc. Natl. Acad. Sci. USA* **2004**, *101*, 15949–15954. [[CrossRef](#)] [[PubMed](#)]
53. Kitamura, T.; Kitamura, Y.I.; Funahashi, Y.; Shawber, C.J.; Castrillon, D.H.; Kollipara, R.; DePinho, R.A.; Kitajewski, J.; Accili, D. A Foxo/Notch pathway controls myogenic differentiation and fiber type specification. *J. Clin. Investig.* **2007**, *117*, 2477–2485. [[CrossRef](#)]
54. Han, C.; Guo, L.; Sheng, Y.; Yang, Y.; Wang, J.; Gu, Y.; Li, W.; Zhou, X.; Jiao, Q. FoxO1 regulates TLR4/MyD88/MD2-NF-kappaB inflammatory signalling in mucosal barrier injury of inflammatory bowel disease. *J. Cell Mol. Med.* **2020**, *24*, 3712–3723. [[CrossRef](#)]
55. Khan, N.; Asif, A.R. Transcriptional regulators of claudins in epithelial tight junctions. *Mediat. Inflamm.* **2015**, *2015*, 219843. [[CrossRef](#)]
56. Wang, Y.; Tong, J.; Zou, D.; Chang, B.; Wang, B.; Wang, B. Elevated expression of forkhead box protein O1 (FoxO1) in alcohol-induced intestinal barrier dysfunction. *Acta Histochem.* **2013**, *115*, 557–563. [[CrossRef](#)]

57. Beard, R.S., Jr.; Haines, R.J.; Wu, K.Y.; Reynolds, J.J.; Davis, S.M.; Elliott, J.E.; Malinin, N.L.; Chatterjee, V.; Cha, B.J.; Wu, M.H.; et al. Non-muscle Mlck is required for beta-catenin- and FoxO1-dependent downregulation of Cldn5 in IL-1beta-mediated barrier dysfunction in brain endothelial cells. *J. Cell Sci.* **2014**, *127*, 1840–1853. [[CrossRef](#)]
58. Wilhelm, K.; Happel, K.; Eelen, G.; Schoors, S.; Oellerich, M.F.; Lim, R.; Zimmermann, B.; Aspalter, I.M.; Franco, C.A.; Boettger, T.; et al. FOXO1 couples metabolic activity and growth state in the vascular endothelium. *Nature* **2016**, *529*, 216–220. [[CrossRef](#)]
59. Li, R.; Ning, Z.; Cui, J.; Khalsa, B.; Ai, L.; Takabe, W.; Beebe, T.; Majumdar, R.; Sioutas, C.; Hsiai, T. Ultrafine particles from diesel engines induce vascular oxidative stress via JNK activation. *Free Radic. Biol. Med.* **2009**, *46*, 775–782. [[CrossRef](#)]
60. Bollati, V.; Marinelli, B.; Apostoli, P.; Bonzini, M.; Nordio, F.; Hoxha, M.; Pegoraro, V.; Motta, V.; Tarantini, L.; Cantone, L.; et al. Exposure to metal-rich particulate matter modifies the expression of candidate microRNAs in peripheral blood leukocytes. *Environ. Health Perspect.* **2010**, *118*, 763–768. [[CrossRef](#)] [[PubMed](#)]
61. Izzotti, A.; Larghero, P.; Balansky, R.; Pfeffer, U.; Steele, V.E.; De Flora, S. Interplay between histopathological alterations, cigarette smoke and chemopreventive agents in defining microRNA profiles in mouse lung. *Mutat. Res.* **2011**, *717*, 17–24. [[CrossRef](#)]
62. Fossati, S.; Baccarelli, A.; Zanobetti, A.; Hoxha, M.; Vokonas, P.S.; Wright, R.O.; Schwartz, J. Ambient particulate air pollution and microRNAs in elderly men. *Epidemiology* **2014**, *25*, 68–78. [[CrossRef](#)]
63. Ooi, A.T.; Ram, S.; Kuo, A.; Gilbert, J.L.; Yan, W.; Pellegrini, M.; Nickerson, D.W.; Chatila, T.A.; Gomperts, B.N. Identification of an interleukin 13-induced epigenetic signature in allergic airway inflammation. *Am. J. Transl. Res.* **2012**, *4*, 219–228. [[PubMed](#)]
64. Taormina, M.J.; Hay, E.A.; Parthasarathy, R. Passive and Active Microrheology of the Intestinal Fluid of the Larval Zebrafish. *Biophys. J.* **2017**, *113*, 957–965. [[CrossRef](#)] [[PubMed](#)]
65. Candeo, A.; Sana, I.; Ferrari, E.; Maiuri, L.; D’Andrea, C.; Valentini, G.; Bassi, A. Virtual unfolding of light sheet fluorescence microscopy dataset for quantitative analysis of the mouse intestine. *J. Biomed. Opt.* **2016**, *21*, 56001. [[CrossRef](#)]
66. Wiles, T.J.; Jemielita, M.; Baker, R.P.; Schlomann, B.H.; Logan, S.L.; Ganz, J.; Melancon, E.; Eisen, J.S.; Guillemin, K.; Parthasarathy, R. Host Gut Motility Promotes Competitive Exclusion within a Model Intestinal Microbiota. *PLoS Biol.* **2016**, *14*, e1002517. [[CrossRef](#)] [[PubMed](#)]
67. Wang, Z.; Zhang, H.; Yang, Y.; Li, Y.; Gao, S.; Fei, P. Deep learning light field microscopy for rapid four-dimensional imaging of behaving animals. *bioRxiv* **2018**. [[CrossRef](#)]

Publisher’s Note: MDPI stays neutral with regard to jurisdictional claims in published maps and institutional affiliations.



© 2020 by the authors. Licensee MDPI, Basel, Switzerland. This article is an open access article distributed under the terms and conditions of the Creative Commons Attribution (CC BY) license (<http://creativecommons.org/licenses/by/4.0/>).